

Accretion disks around black holes: dynamical evolution, meridional circulations and gamma ray bursts

William H. Lee

*Instituto de Astronomía, Universidad Nacional Autónoma de México,
Apdo. Postal 70-264, Cd. Universitaria, México D.F. 04510*

and

Enrico Ramirez-Ruiz

*Institute of Astronomy,
Madingley Road, Cambridge, CB30HA, U.K.*

ABSTRACT

We study the hydrodynamical evolution of massive accretion disks around black holes, formed when a neutron star is disrupted by a black hole in a binary system. The initial conditions are taken from three-dimensional calculations of coalescing binaries. By assuming azimuthal symmetry we are able to follow the time dependence of the disk structure for 0.2 seconds in cylindrical coordinates (r, z) . We use an ideal gas equation of state, and assume that all the dissipated energy is radiated away. The disks evolve due to viscous stresses, modeled with an α -law. We study the disk structure, and in particular the strong meridional circulations that are established and persist throughout our calculations. These consist of strong outflows along the equatorial plane that reverse direction close to the surface of the disk and converge on the accretor. In the context of gamma ray bursts (GRBs), we estimate the energy released from the system in neutrinos and through magnetic-dominated mechanisms, and find it can be as high as $E_\nu \approx 10^{52}$ erg and $E_{BZ} \approx 10^{51}$ erg respectively, during an estimated accretion timescale of 0.1–0.2 seconds. $\nu\bar{\nu}$ annihilation is likely to produce bursts from only a short, impulsive energy input $L_{\nu\bar{\nu}} \propto t^{-5/2}$ and so would be unable to account for a large fraction of bursts which show complicated light curves. On the other hand, a gas mass $\approx 0.1 - 0.25M_\odot$ survives in the orbiting debris, which enables strong magnetic fields $\approx 10^{16}$ G to be anchored in the dense matter long enough to power short duration GRBs. We highlight the effects that the initial disk and

black holes masses, viscosity and binary mass ratio have on the evolution of the disk structure. Finally, we investigate the continuous energy injection that arises as the black hole slowly swallows the rest of the disk and discuss its consequences on the GRB afterglow emission.

Subject headings: accretion, accretion disks — hydrodynamics — gamma rays: bursts

1. Introduction

Accretion onto black holes has been considered as an efficient way to transform gravitational energy into radiation (Salpeter 1964; Zel’dovich 1964), and is often thought to occur in the form of a disk, due to the angular momentum of the accreting matter. This almost certainly is the case in a variety of astrophysical systems, ranging from AGNs with very massive black holes to stellar mass binaries, analogous to the X-ray binaries known to contain neutron stars (King 1995). The flows in these disks may exhibit very different morphologies depending on the physical conditions present in the system. Accretion is generally thought to proceed through the transport of angular momentum from the inner to the outer regions of the disk, although the mechanism by which this is accomplished is not entirely clear. The parametrization introduced by Shakura & Sunyaev (1973) has allowed much progress to be made, without specifying the physics behind the viscosity responsible for angular momentum transport. Magnetohydrodynamical studies (analytical and numerical) appear to indicate that magnetic fields and their associated instabilities in disks can effectively generate a viscosity that would drive their evolution (Balbus & Hawley 1991; Hawley & Balbus 1991; Hawley 2000; Stone & Pringle 2001; Hawley & Krolik 2001, 2002), with equivalent values for the α parameter in the range 0.01–0.1 (Balbus & Hawley 1998). Additionally, it has become clear that hydrodynamic processes can play an important role in the structure and evolution of disks, and that multi-dimensional, time-dependent computations are necessary to fully understand these effects, particularly since the flows can be quite complicated, often exhibiting strong variability, and composed of combinations of inflows/outflows of varying intensity (Igumenshchev 2000).

In this context we are motivated to study accretion disks around black holes hydrodynamically, particularly in what concerns central engines for cosmological gamma ray bursts (GRBs). The energetics of GRBs ($10^{50} - 10^{52}$ erg are typically released in a few seconds) and the variability shown in their lightcurves (down to millisecond timescales) argues in favor of a compact source that produces a relativistic outflow, usually referred to as a fireball (Rees & Mészáros 1992). The complicated light curves can then be understood in terms of internal

shocks in the outflow itself, caused by velocity variations in the expanding plasma (Rees & Mészáros 1994; Sari & Piran 1997; Fenimore, Ramirez-Ruiz & Wu 1999; Ramirez-Ruiz & Fenimore 2000; Nakar & Piran 2002). The durations range from 10^{-3} s to about 10^3 s, with a bimodal distribution of short ($\simeq 0.2$ s) and long bursts ($\simeq 40$ s) (Kouveliotou et al. 1993; Norris et al. 1996). One possible scenario, at least for the class of short bursts¹, involves the coalescence of compact binaries containing a black hole (BH) and a neutron star (NS), or two neutron stars (Lattimer & Schramm 1976; Paczyński 1986, 1991; Eichler et al. 1989; Narayan, Paczyński & Piran 1992; Mochkovitch et al. 1993; Katz & Canel 1996; Kluźniak & Lee 1998; Popham, Woosley & Fryer 1999; Ruffert & Janka 1999; Rosswog & Davies 2002). Such systems do exist, like PSR1913+16 (Hulse & Taylor 1975), and they will coalesce due to angular momentum losses to gravitational radiation, provided that the orbital separation is small enough. The binary coalescence rates are in rough agreement with the observed GRB rate (Kalogera et al. 2001). The typical dynamical timescale in such binaries immediately prior to coalescence (\approx ms) is much shorter than the observed burst duration, and so it requires that the central engine evolves into a configuration that is stable, while retaining a sufficient amount of energy to power the burst.

The formation of a BH with a debris torus around it is a common ingredient of both these scenarios, whose accretion can provide the release of sufficient gravitational energy $\approx 10^{54}$ erg to power a GRB (Rees 1999). A fireball arises from the large compressional heating and dissipation associated with this accretion, which can provide the driving stress necessary for relativistic expansion (Piran 1999; Mészáros 2001). Possible forms of this outflow are kinetic energy of relativistic particles generated by $\nu\bar{\nu}$ annihilation or an electromagnetic Poynting flux.

In either mechanism, the duration of the burst is determined by the viscous timescale of the accreting gas², which is significantly longer than the dynamical timescale, thus accounting naturally for the large difference between the durations of bursts and their fast variability. Any instability (of hydrodynamical or magnetic origin) would presumably be reflected in the relativistic outflow. Strong magnetic fields anchored in the dense matter surrounding the BH would produce large amplitude variations in the energy release (Usov 1992; Mészáros & Rees 1997). A weaker field would extract inadequate power; on the other hand a neutron torus, with its huge amount of differential rotation, is a natural site for the onset of a dynamo process that winds up the magnetic field to the required intensity

¹We note, furthermore, that those with detected afterglows are all in the long category (although see Lazzati, Ramirez-Ruiz & Ghisellini (2001) and Connaughton (2002)).

²In the collapsar scenario, the burst duration is given by the fall-back time of the gas (Woosley 1993; MacFadyen & Woosley 1999)

(Usov 1994; Kluźniak & Ruderman 1998). An acceptable model requires that the orbiting debris not be dispersed completely on too short a timescale, lasting at least as long as the characteristic duration of the burst. The tidal disruption of a neutron star by a black hole would redistribute matter and angular momentum very rapidly. The key issue is then how long a sufficient amount of this matter survives to power a burst.

In this paper, we study the evolution of realistic disks resulting from dynamical coalescence calculations (see below §2), on timescales that are comparable to the durations of short GRBs (i.e. a few tenths of a second). Recently, the steady state structure of similar disks has been examined by Narayan, Piran & Kumar (2001) and Kohri & Mineshige (2002). Since we wish to investigate the evolution of the disk and its stability, no steady state assumptions are made regarding its structure. This allows us to compare the strength of the energy release by $\nu\bar{\nu}$ annihilation relative to MHD coupling and to investigate their potential as a viable source for GRB production.

The hydrodynamics of black hole–neutron star coalescence has been considered in detail by Lee & Kluźniak (1999a,b) and Lee (2000, 2001a), using an ideal gas equation of state and varying its stiffness through the adiabatic index Γ . The simulations explored the effect of different initial binary mass ratios $q_b = M_{\text{NS}}/M_{\text{BH}}$ and the spin configuration of the neutron star, with respect to the orbital motion. The viscosity inside neutron stars is far too small to permit synchronization during the inspiral phase (Kochanek 1992; Bildsten & Cutler 1992), so it is reasonable to assume that the neutron star spin is negligible with respect to the orbital angular momentum. The exact equation of state at supra–nuclear densities is uncertain, but it would appear that the radius is largely independent of the mass (Lattimer & Prakash 2001), so that in the polytropic approximation, one would assume $\Gamma = 2$. Coalescence calculations with this set of parameters were computed by Lee (2001a, hereafter L01). In particular, we will use here the results of runs C50 and C31 in that paper, with $q_b = 0.5$ and $q_b = 0.31$ respectively (both runs used an index $\Gamma = 2$).

2. Numerical method and implementation

The equations of hydrodynamics are solved in two dimensions using Smooth Particle Hydrodynamics (SPH) (Monaghan 1992). Three–dimensional dynamical coalescence calculations are only followed for a few tens of milliseconds, at most (those in L01 spanned 23 ms), because of computational limitations. Since we wish to explore the behavior of the accretion structures on timescales that are much longer than the dynamical one, we have assumed azimuthal symmetry in the system, and mapped the output from the 3D calculations to

cylindrical (r, z) coordinates. This allows us to follow the calculations for a few tenths of a second (all the runs shown in this paper were terminated at $t = 0.2$ s). We have not assumed reflection symmetry with respect to the equatorial ($z = 0$) plane.

We use a simple ideal gas equation of state, with $P = \rho u(\Gamma - 1)$ (u is the internal energy per unit mass), and the fluid is initially given the azimuthal velocity v_ϕ required for centrifugal equilibrium. The self-gravity of the disk is neglected, and the black hole produces a Newtonian point-mass potential $\Phi_{\text{BH}} = -GM_{\text{BH}}/r$. Accretion is modeled by an absorbing boundary at $r_{\text{Sch}} = 2GM_{\text{BH}}/c^2$. In practice, only the inner regions of the 3D disk are mapped onto two dimensions to start the calculation (with $0 < |z| < 200$ km and $0 < r < 400$ km).

The above simplifications clearly do not correspond to the physical conditions one would encounter in such a disk, but we have chosen to use them as a first approximation to the solution for several reasons. In the first place, the 3D dynamical calculations that gave rise to the disks we now use as initial conditions were fully Newtonian (except for the inclusion of gravitational radiation reaction terms), particularly regarding the form of the gravitational potential produced by the black hole. For consistency we have thus kept this form. In the future we will explore situations in which the black hole potential is given by a form which reproduces the effects of a marginally stable orbit (e.g. that of Paczyński & Wiita (1980)). Second, the equation of state was likewise very simple in the initial calculations, and we have maintained it in the present work. The only change we apply is that at $t = 0$ the value of the index Γ has been lowered for some runs (see Table 1) from 2 to 4/3. We will also improve on the form of the equation of state in future simulations. Third, the final conditions of the 3D calculations show that the self-gravity of the disk is not too important in determining its structure (it is pressure support that makes the rotation curve deviate from what would be expected for point masses orbiting a massive body, see e.g. Figure 8b in L01).

The second important new ingredient (the first one being the assumption of azimuthal symmetry) in the present simulations is the transport of angular momentum by viscosity, which is modeled by including all the terms derived from the stress tensor $t_{\alpha\beta}$ in the equations of motion (we use the formalism developed by Flebbe et al. (1994)). We have:

$$\frac{dv_\alpha}{dt} = -\frac{P_{,\alpha}}{\rho} - \Phi_{\text{BH},\alpha} + \frac{t_{\alpha\beta,\beta}}{\rho} + \left(\frac{dv_\alpha}{dt}\right)_{\text{art}} \quad (1)$$

where the commas indicate partial derivatives. The last term arises from the presence of artificial viscosity (see below). The tensor responsible for the viscous force is $t_{\alpha\beta}$, given by:

$$t_{\alpha\beta} = \eta(v_{\alpha,\beta} + v_{\beta,\alpha} - \frac{2}{3}\delta_{\alpha\beta}v_{\gamma,\gamma}), \quad (2)$$

where η is the dynamical viscosity coefficient, and the shear is:

$$\sigma_{\alpha\beta} = v_{\alpha,\beta} + v_{\beta,\alpha} - \frac{2}{3}\delta_{\alpha\beta}v_{\gamma,\gamma} \quad (3)$$

The energy dissipation per unit mass is:

$$T\frac{ds}{dt} = \frac{\eta}{2\rho}\sigma_{\alpha\beta}\sigma_{\alpha\beta} + \left(T\frac{ds}{dt}\right)_{art} \quad (4)$$

To perform a dynamical calculation, at this point one needs to fix a prescription for the viscosity. We have chosen to parametrize its magnitude by using an α -law, setting $\eta = \alpha\rho c_s^2/\Omega_k$, where $c_s = (\Gamma P/\rho)^{1/2}$ is the adiabatic sound speed and Ω_k is the Keplerian angular velocity. This formulation of the viscosity has been used before in time-dependent studies of accretion flows in two and three dimensions (Igumenshchev, Chen & Abramowicz 1996; Igumenshchev & Abramowicz 1999, 2000; Igumenshchev, Abramowicz & Narayan 2000; McKinney & Gammie 2002). We note that the simulations reported here are followed for a timescale that is much longer than the viscous one, and thus solutions that are qualitatively steady are obtained in all cases (they cannot be steady quantitatively simply because there is no external agent feeding the disk with matter as the simulation progresses).

The implementation of SPH for the present 2D azimuthally symmetric calculations requires the writing of the above expressions in cylindrical coordinates. For completeness, we give here the full set of equations for momentum and energy:

$$\frac{dv_r}{dt} = -\frac{1}{\rho}\frac{\partial P}{\partial r} - \frac{GM_{\text{BH}}r}{R^3} + \frac{1}{\rho}\left(\frac{\partial t_{rr}}{\partial r} + \frac{t_{rr}}{r} + \frac{\partial t_{rz}}{\partial z}\right) + \left(\frac{dv_r}{dt}\right)_{art} \quad (5)$$

$$\frac{dv_\phi}{dt} = \frac{1}{\rho}\left(\frac{2t_{r\phi}}{r} + \frac{\partial t_{\phi r}}{\partial r} + \frac{\partial t_{\phi z}}{\partial z}\right) \quad (6)$$

$$\frac{dv_z}{dt} = -\frac{1}{\rho}\frac{\partial P}{\partial z} - \frac{GM_{\text{BH}}z}{R^3} + \frac{1}{\rho}\left(\frac{\partial t_{zr}}{\partial r} + \frac{t_{zr}}{r} + \frac{\partial t_{zz}}{\partial z}\right) + \left(\frac{dv_z}{dt}\right)_{art} \quad (7)$$

$$\frac{du}{dt} = -\left(\frac{P}{\rho}\right)\nabla\cdot\vec{v} + T\frac{ds}{dt} \quad (8)$$

Here $R = \sqrt{r^2 + z^2}$ is the distance to the origin, and the artificial viscosity terms are computed using the prescription of Balsara (1995) to minimize the effects of artificial shear on the evolution of the disk. The explicit forms of the acceleration and the energy dissipation for a given SPH particle are:

$$\left(\frac{d\vec{v}}{dt}\right)_{i,art} = -\sum_{j\neq i} m_j \Pi_{ij} \nabla_i W_{ij}, \quad (9)$$

and

$$\left(T \frac{ds}{dt}\right)_{i,art} = \frac{1}{2} \sum_{j \neq i} m_j \Pi_{ij} (\vec{v}_i - \vec{v}_j) \cdot \nabla_i W_{ij}, \quad (10)$$

where W is the SPH interpolation kernel given by Monaghan & Lattanzio (1985), adapted to azimuthal symmetry:

$$W(r, h) = \frac{10}{7\pi h^2} \frac{1}{(2\pi r)} \begin{cases} 1 - 3(r/h)^2/2 + 3(r/h)^3/4, & 0 \leq r/h < 1, \\ (2 - r/h)^3/4, & 1 \leq r/h < 2, \\ 0, & 2 \leq r/h. \end{cases} \quad (11)$$

We have

$$\Pi_{ij} = \left(\frac{P_i}{\rho_i^2} + \frac{P_j}{\rho_j^2} \right) (-\alpha_b \mu_{ij} + \beta_b \mu_{ij}^2), \quad (12)$$

where

$$\mu_{ij} = \begin{cases} \frac{(\mathbf{v}_i - \mathbf{v}_j) \cdot (\mathbf{r}_i - \mathbf{r}_j)}{h_{ij}(|\mathbf{r}_i - \mathbf{r}_j|^2/h_{ij}^2) + \eta^2} \frac{f_i + f_j}{2c_{ij}}, & (\mathbf{v}_i - \mathbf{v}_j) \cdot (\mathbf{r}_i - \mathbf{r}_j) < 0 \\ 0, & (\mathbf{v}_i - \mathbf{v}_j) \cdot (\mathbf{r}_i - \mathbf{r}_j) \geq 0 \end{cases}$$

and f_i is the form-function for particle i defined by

$$f_i = \frac{|\nabla \cdot \mathbf{v}|_i}{|\nabla \cdot \mathbf{v}|_i + |\nabla \times \mathbf{v}|_i + \eta' c_i / h_i}.$$

The factor $\eta' \simeq 10^{-4}$ in the denominator prevents numerical divergences. The smoothing length and sound speed for particle i are denoted by h_i and c_i respectively, and α_b and β_b are constants of order unity (we use $\alpha_b = \beta_b = \Gamma/2$). The number of neighbors for the hydrodynamical interpolation is kept fixed at $\nu = 24$.

Artificial viscosity is used in SPH to model the presence of shocks and avoid particle inter-penetration. The forms initially employed have been substantially improved over the years, with an accompanying reduction in spurious numerical effects. Most notably, the one we use here is such that the shear viscosity is suppressed when the compression in the fluid is low and the vorticity is high ($|\nabla \times \vec{v}| \gg |\nabla \cdot \vec{v}|$, as is the case in accretion disks with differential rotation), but remains in effect if compression dominates in the flow ($|\nabla \cdot \vec{v}| \gg |\nabla \times \vec{v}|$).

We are able to monitor just how important the dissipation due to artificial viscosity is, compared with that arising from the stress tensor $t_{\alpha\beta}$ (see equation 4). We employed two different values of the viscosity parameter α for the runs shown here (see Table 1): $\alpha = 0.1$ and $\alpha = 0.01$. For both cases, the energy dissipated through artificial viscosity is most

important at early times ($t < 10$ ms), and quickly decreases relative to the terms generated through $t_{\alpha\beta}$ (see below, §3).

We have tested our code to ensure that the viscous terms are computed correctly. The most simple test is to calculate the spreading of a ring of gas due to viscosity (with no vertical structure) orbiting a point mass, when pressure effects and self-gravity are neglected. This problem has an analytic solution in terms of Bessel functions (Pringle 1981), which can be easily compared with a numerical solution. Our code reproduces this calculation accurately, with the ring spreading radially on the correct timescale.

We have also performed a second class of tests, allowing for vertical structure in azimuthal symmetry, studying the evolution of thick tori, where pressure effects are important and self-gravity is neglected. Two different types of calculations were performed. In the first, a torus in hydrostatic equilibrium around a black hole, with an initially specified distribution of specific angular momentum, was allowed to evolve, switching the viscosity on at the start of the calculation (Igumenshchev, Chen & Abramowicz 1996). In the second, a continuous flow of matter was injected at a large radius, and a disk was formed on the viscous timescale (Igumenshchev & Abramowicz 1999). For each of these, several values of the α parameter were used, ranging from 10^{-3} to 10^{-1} . We found excellent agreement with previously published results, both qualitatively and quantitatively (Lee 2001b).

Finally, we assume that all the energy dissipated in the flow is radiated away in neutrinos, and thus in this respect, the flow is an NDAF (Neutrino Dominated Accretion Flow), as done by Narayan, Piran & Kumar (2001) and Kohri & Mineshige (2002). This is accomplished by directly removing from the fluid the internal energy associated with the first term in equation (4). The neutrino luminosity is then given by $L_\nu = \int \eta \sigma_{\alpha\beta} \sigma_{\alpha\beta} / 2\rho \, dm$. The energy dissipated by artificial viscosity remains in the disk as internal energy. This is another aspect that clearly needs to be treated in a more realistic manner and will be dealt with in future work.

3. Results

3.1. Structure and fluid circulation in the disks

The choice of parameters shown in Table 1 for the simulations allows us to explore the effect of numerical resolution on the results (runs D and E, and runs F and G differ only in the initial number of particles), as well as that of the magnitude of the viscosity, the compressibility of the gas in the disk, and the initial mass of the black hole. For a lower black hole mass M_{BH} the accretion disk is initially more massive, and the spin angular momentum

of the black hole is larger. This is a reflection of the previous binary evolution and tidal disruption that led to the formation of the accretion disk.

The initial conditions we have used for the accretion disks clearly do not correspond to a simple equilibrium configuration, since they are derived from three-dimensional dynamical calculations. In our case, the disks are initially hot (the internal energy is about 10 MeV/nucleon, see Figure 8 in L01), and thus pressure support is important, making them quite thick ($H/R \approx 0.5$). This energy reservoir is not entirely lost, since only the energy dissipated through the physical viscosity is radiated away in neutrinos. Thus the disks remain thick throughout the dynamical evolution.

All the dynamical calculations are qualitatively similar. We show snapshots of the density and velocity field in the disk at various times for runs E ($\alpha = 0.1$) and G ($\alpha = 0.01$) in Figures 1 and 2. At the start of the calculation, the disk flattens slightly, on a vertical free-fall timescale $t_{ff} \approx \sqrt{r^3/GM_{\text{BH}}} \approx 1 - 2$ ms, since it is not in strict hydrostatic equilibrium at $t = 0$. The initial panels (at $t = 10$ ms) show the formation of a weak shock at $r \simeq 140$ km, formed when the outer regions of the torus move radially inwards. This front moves subsequently outwards, and has practically left the inner region of the disk by $t = 20$ ms. Thereafter accretion proceeds onto the black hole in a characteristic pattern, which is mainly dependent on the value of α .

The simulations use a variable smoothing length h to ensure an accurate interpolation of the fluid variables, and so the spatial resolution (which is essentially equal to h), is also variable. It is smallest in the regions of highest density (in the midplane of the disk). At $t = 0.1$ s, the smallest scales that can be resolved are of order 2×10^4 cm = 200 m at $r \simeq 30$ km, and 3×10^5 cm = 3 km close to the surface of the disk (where $\rho \simeq 10^9$ g cm $^{-3}$ for the high-resolution runs E and G; in two dimensions the smoothing length scales with the number of particles as $h \propto N^{-1/2}$). The circulation patterns seen in Figure 2 are much larger than the spatial resolution and thus are clearly resolved. The runs with a lower number of particles have a slightly poorer resolution, but nevertheless resolve the same global features clearly in terms of accretion rate, spatial extension of the disk and circulation patterns.

For a high viscosity, a large-scale circulation is established, with $z \approx r$. There is outflow in the equatorial plane at large distances from the black hole, and accretion takes place only along the surface of the disk and in the equatorial plane quite close to the black hole ($r \simeq 50$ km). The radial velocities are subsonic, and the turnaround in v_r occurs in large eddies close to the surface of the disk, when the gas is moving away from the equatorial plane. The disk slowly spreads in the radial direction, with an accompanying drop in density and accretion rate (at $t = 0.2$ s, \dot{M} has dropped by about one order of magnitude compared to its value at 10 ms, see also Figure 7a below).

For the low viscosity case, the flow is more complicated. Accretion onto the black hole still occurs only along the surface of the disk and in the equatorial plane at small values of r . However, the circulation patterns are present on smaller scales than before, with $z < r$. The flow is qualitatively steady after approximately 20 ms, but the eddies persist throughout the simulation. The radial spread of the disk is less pronounced than before, due to the lower value of α , and thus higher densities are maintained for a longer period. The accretion rate onto the black hole is about one order of magnitude lower (for $t < 20$ ms) than for the high viscosity runs, and decreases more slowly.

The circulation patterns described above can be clearly related to the distribution of specific angular momentum l in the disk. We show in Figure 3 the contours of l for runs E and G at $t = 40$ ms. As one moves from the equator (where $v_r > 0$) to the surface of the disk at a given value of r , l decreases until the fluid turns around and flows inward.

For both cases, the magnitude of the velocities (radial and vertical) in the disk decreases in time, with the circulation patterns becoming less intense in that respect. Figure 4 shows views of the disks for runs E and G at $t = 0.11$ s on a larger scale.

The mass accretion rate onto the black hole is clearly sensitive to the value of α , and to a lesser extent, on the adiabatic index Γ , as can be seen in Figure 7a. Runs E and G differ only in the value of α , and clearly lowering the viscosity leads to less vigorous transport of angular momentum, and thus to a reduced \dot{M}_{BH} . Runs E and C differ only in the value of Γ . The less compressible case (run C, with $\Gamma = 2$) has a broader spatial mass distribution and reaches lower peak densities. Thus slightly more mass is initially closer to the accretor and easily absorbed, giving a larger \dot{M}_{BH} , and subsequently a faster drop (by $t = 0.2$ s, the disk mass is lower in run C than in run E, see Table 2). Finally, run B differs from run E in the initial binary system that gave rise to the accretion disk, with a larger M_{BH} and smaller M_{disk} , which is responsible for the lower accretion rate.

Meridional circulation patterns like the ones seen in the present simulations have been studied before, both analytically and numerically. Solving for the vertical structure of an accretion disk and using an α viscosity, Urpin (1984) found that the radial flow can change direction in the midplane of the disk, with $v_r > 0$. Kita (1995) and Kluźniak & Kita (2000) assumed a steady state in a polytropic α -disk and found solutions which exhibited outflow along the equator, with inflow along the disk surface and in the equator close to the accretor, as seen here. In their study it was the value of α that fixed the equatorial distance at which the flow turned from inflow to outflow (the stagnation radius). In both cases, the authors assumed that the disk cools efficiently, with the dissipated energy being radiated away.

To our knowledge, numerical work has been performed so far mainly with Eulerian codes,

in which boundary conditions need to be specified. Kley & Lin (1992) obtained outflow in the midplane of the disk, and inflow along the surface, as in the solution found by Urpin (1984), but the use of height-averaged boundary conditions enforced artificial circulation at the edges of the computational domain, thus altering the flow structure substantially. In other cases, a free outflow condition is used, meaning that gas which leaves the computational domain cannot re-enter it at a later time. These calculations — which, contrary to what we have assumed, suppose that the dissipated energy is advected with the flow — have also revealed circulation patterns and inflows/outflows with morphologies that depend on the magnitude of the viscosity (Igumenshchev & Abramowicz 1999; Stone, Pringle & Begelman 1999; McKinney & Gammie 2002).

The use of SPH is clearly an advantage in this sense, since there are no boundary conditions at all and the modeling of the fluid is not restricted to a particular region in space.

3.2. Dynamical stability

There are several instabilities that can affect massive accretion disks dynamically and shorten their lifetimes considerably, compared with the viscous timescale. One of these is the “runaway radial” instability, first discussed in the context of massive accretion disks at the centers of galaxies (Abramowicz et al. 1983). A number of different effects can work to enhance or suppress this phenomenon, namely (i) the spin of the black hole, (ii) the distribution of angular momentum in the disk, given by $l \propto r^p$, (iii) the effects of general relativity and (iv) the self-gravity of the disk. The first two (large Kerr parameter and a high value of p) tend to suppress the instability (Wilson 1984; Daigne & Mochkovitch 1997; Abramowicz, Karas & Lanza 1998; Masuda, Nishida & Eriguchi 1998; Lu et al. 2000), while the others tend to enhance it (Nishida et al. 1996; Nishida & Eriguchi 1996; Masuda, Nishida & Eriguchi 1998; Font & Daigne 2002). The numerical approach used here allows us only to comment on (ii). The distribution of angular momentum in the disk can be approximated by a power law in the three-dimensional SPH coalescence simulations, with $l \propto r^{0.45}$, i.e. quite close to Keplerian (see Figures 10b and 8b in Lee (2000) and L01 respectively). This does not vary appreciably as the calculations progress, despite the circulation of the fluid in the disk described above in §3.1, and thus we find that the disk is stable in this respect.

Additionally, disks can be unstable to axisymmetric perturbations depending on their surface density and temperature (measured through the sound speed c_s). This is known as Toomre’s stability criterion, and can be quantified through $Q = c_s \kappa / \pi G \Sigma$, where κ is the

local epicyclic frequency and Σ is the mass surface density:

$$\Sigma(r) = \int_{-\infty}^{\infty} \rho(r, z) dz. \quad (13)$$

For $Q > 1$ the disk is stable to axisymmetric perturbations, and unstable otherwise. This condition tells us that a dense, cold disk is more likely to be unstable than a hot, thick one (such as the ones treated here). We find that for all our runs, $Q > 1$. The profile of Q is such that at a given instant in time, there is a minimum Q_{min} at a certain radius (close to the maximum in density, see Figure 5). The lowest value of Q_{min} occurs at $t = 0$, where $(r_Q, Q_{min}) \approx (50 \text{ km}, 5)$. As the disk evolves, the density drops and both parameters increase. By $t = 0.2 \text{ s}$, we typically find $(r_Q, Q_{min}) \approx (150 \text{ km}, 10)$.

3.3. Relative importance of artificial viscosity

The artificial viscosity mentioned above in §2 ideally should not affect the accretion flow substantially, otherwise the results would be difficult to assess. As a measure of the effect the terms arising from it have on the disk, we plot in Figure 6 the dissipated energy as a function of time, separated into the components arising from $t_{\alpha\beta}$ and those coming from artificial viscosity, for runs E and G (the former is in fact what we have termed the neutrino luminosity L_ν above in §2). It is at early times ($t < 10 \text{ ms}$) that artificial viscosity is important. This is not surprising, since that is when the initial transient appears in the disk and the shock forms at $r \approx 140 \text{ km}$. Thus the relative importance of the artificial viscosity merely means that it is working as one would expect. After this transient dies out, the dissipation rate becomes quickly dominated by the physical viscosity. It is also apparent that only for low values of α (run G with $\alpha = 0.01$) are the two terms comparable in magnitude in the initial stages. We are thus confident that our results are not affected significantly by the presence of artificial viscosity.

4. Summary and discussion

We have computed the dynamical evolution of massive accretion disks around stellar-mass black holes in two dimensions (with azimuthal symmetry), formed through the tidal disruption of a neutron star by a black hole in a close binary ($M_{\text{BH}} \approx 4M_\odot$ and $M_{\text{disk}} \approx 0.3M_\odot$). Our initial conditions are taken from the final state of three dimensional hydrodynamical calculations of the coalescence process, by averaging in the azimuthal direction. We use Newtonian physics, an ideal gas equation of state, and solve the equations of viscous hydrodynamics assuming an α law for the viscosity coefficient. All the energy dissipated by

the physical viscosity is radiated away (in neutrinos). The time evolution is followed for 0.2 seconds.

We find that after an initial transient of numerical origin, stemming from the fact that the 3D torus does not exhibit strict azimuthal symmetry due to the highly dynamical merging process (see Figures 2 and 7 in L01), the disk settles to a qualitatively steady state. Meridional circulations are promptly established, whose structure depends mainly on the value of the α parameter. Most strikingly, there is an important motion of fluid from the inner regions of the disks to large radii, along the equatorial plane. The flow is directed towards the accreting black hole along the surface of the disk and in the equatorial region at small radii. The disks remain thick ($H/R \simeq 0.5$) throughout the dynamical evolution, due to their large internal energy, with accretion rates on the order of one solar mass per second. The maximum densities decrease during our calculations, as there is no external agent feeding the disks, but remain at $\simeq 10^{12}$ g cm $^{-3}$, with corresponding internal energy densities $\simeq \text{few} \times 10^{30}$ erg cm $^{-3}$.

We stress that the evolution of accretion disks such as these should be studied with time-dependent models, since the system is clearly not in a steady state, even from its inception. The circulation pattern seen in Figure 2 would certainly lengthen their lifetimes by moving matter to larger radii continuously, an effect that would otherwise be omitted. To illustrate how important this can be, we considered the total radial mass flux in the disk, composed of two parts at any given value of the radial coordinate r , $\dot{M}(r) = \dot{M}_{in}(r) + \dot{M}_{out}(r)$ where

$$\dot{M}_{in} = 2\pi r \int_{v_r < 0} \rho v_r dz, \quad \dot{M}_{out} = 2\pi r \int_{v_r > 0} \rho v_r dz, \quad (14)$$

restricted to regions in which $v_r < 0$ for \dot{M}_{in} and $v_r > 0$ for \dot{M}_{out} respectively. By definition, $\dot{M}_{in} < 0$ and $\dot{M}_{out} > 0$. If there were no circulation in the disk and all matter moved radially inward one would have $\dot{M}_{out} = 0$ and $\dot{M} = \dot{M}_{in} < 0$. A measure of how important the circulations are, and how much they would lengthen the lifetime of the disks can be obtained by calculating the fraction of the gas flowing radially in the disk that is actually moving toward the accretor, i.e. $|\dot{M}_{in}|/(|\dot{M}_{in}| + |\dot{M}_{out}|)$. In the inner regions of the disks this ratio tends to unity, as can be seen from Figure 2. It decreases rapidly at larger radii, reaching about 1/3 for run E and 1/10 for run G at $r \simeq 100$ km midway through the simulations (at $t = 0.1$ s). Thus most of the radial flow of gas actually cancels out in the circulations, with a residual amount left over moving toward the black hole.

We now turn to the implications our calculations might have on models for the production of cosmological gamma ray bursts from coalescing compact binaries. The two main forms of energy release from the disk we consider are i) neutrino emission and ii) MHD flow, either through the Blandford–Znajek effect (Blandford & Znajek 1977) or by means of a

magnetized wind.

In the first case, we make a rough estimate for L_ν and E_ν from the dissipated energy because of viscosity (see Table 2), as mentioned above. We have made an estimate only for the total neutrino luminosity L_ν , and not for the *annihilation* luminosity $L_{\nu\bar{\nu}}$, which would determine if a relativistic fireball could be launched or not. The calculation of $L_{\nu\bar{\nu}}$ requires the use of a more realistic equation of state, which we will explore in future work. For the time being, we note that, regardless of the efficiency of energy conversion from neutrino luminosity to annihilation luminosity — which could be quite low, on the order of 1 per cent or less (Ruffert & Janka 1999; Popham, Woosley & Fryer 1999)— it appears that the time-dependence of L_ν , which follows that of \dot{M}_{BH} (see Figure 7a and Table 2), is such that neutrinos could only be responsible for a very short, almost impulsive energy release ($L_\nu \propto t^{-5/4}$, so $L_{\nu\bar{\nu}} \propto L_\nu^2 \propto t^{-5/2}$), and thus would be unable to power a burst lasting several tenths of a second or more. Of course this does not mean that it would have a negligible impact on the structure of the burst itself. We note furthermore that in the detailed 3D calculations done by Ruffert & Janka (1999) for the evolution of thick disks following the coalescence of two neutron stars, the “neutrinosphere” is quite close to an isodensity surface at $\rho = 10^{11} \text{ g cm}^{-3}$, which is lower than the maximum densities present in the disks computed here, even at late times (see Figures 1 and 4). Rosswog & Davies (2002) have also performed 3D calculations of binary neutron star coalescence taking into account neutrino emission and scattering processes, finding as well that in the regions of highest density the material is opaque, in their case mainly because of scattering off heavy nuclei. Thus it is clear that a complete picture must include an appropriate formulation of neutrino transport.

For the magnetic-dominated case we must make some assumptions, since our simulations do not incorporate the effects of magnetic fields explicitly. For the field to be able to extract the binding energy of the torus, it should be anchored to it, and we assume its magnitude is directly related to the internal energy in the gas. For this purpose we show in Table 2 the internal energy density ρc_s^2 at $t = 0.1 \text{ s}$ in the inner regions of the disk (at $r = 1.25r_{\text{Sch}}$ ($\approx 15 \text{ km}$ for runs A and B, and $\approx 20 \text{ km}$ for runs C through G) in the equatorial plane. It is of order $10^{30} \text{ erg cm}^{-3}$, and even larger for the case with low viscosity ($\alpha = 0.01$). From this we compute an estimate for the Blandford–Znajek luminosity as

$$L_{BZ} \approx 10^{50} a^2 \left(\frac{M_{\text{BH}}}{3 M_\odot} \right)^2 \left(\frac{B}{10^{15} \text{ G}} \right)^2 \text{ erg s}^{-1} \quad (15)$$

where $a \simeq 0.3$ is the Kerr parameter of the black hole and the magnitude of the magnetic field is computed using $B^2/8\pi = \rho c_s^2$ (this gives $B \approx 10^{16} \text{ G}$ in all cases). This is clearly the most optimistic scenario concerning energy release, in that it assumes that the magnetic field strength is at the equipartition value. The time evolution of L_{BZ} is shown in Figure 7b

for several runs. For a larger viscosity, the gas in the disk drains into the black hole on a shorter timescale, and thus the drop in L_{BZ} is much faster than for a low value of α (in run G, $L_{BZ} \approx 5 \times 10^{51}$ erg s $^{-1}$ is practically constant).

In principle, energy can be extracted over many dynamical timescales if magnetic fields can tap the rotational energy of the accretion disk and of the black hole. Here $L_{BZ} \propto (t/t_0)^{q'}$ is the intrinsic luminosity of the central engine measured in the fixed frame, where $-5/4 < q' < 0$ (see Figure 7b). For such a continuously fed fireball, a forward shock propagating into the external medium and a reverse shock moving back into the relativistic outflow will coexist on either side of the contact discontinuity. The latter may persist as long as a significant level of energy injection is maintained. The differential energy conservation relation for the self-similar blast wave can be written as $dE/dt = L_{BZ}(t/t_0)^{q'} - \kappa'(E/t)$ (Cohen, Piran & Sari 1998), where the first term denotes steady energy injection, and the second accounts for possible radiative energy losses of the fireball, with q' and κ' being dimensionless constants. In the adiabatic case (no radiative losses) $\kappa' = 0$ and the Lorentz factor evolves as $\Gamma^2 \propto t^{-3}$ (Blandford & McKee 1976). For $q' \neq -1 - \kappa'$, an analytical solution can be found: $E = [L_{BZ}/(q' + \kappa' + 1)](t/t_0)^{q'} + E_{\text{imp}}(t/t_0)^{-\kappa'}$ for $t > t_0$, where $E_{\text{imp}} = E_{\nu\bar{\nu}}$ describes the impulsive energy input. Here t_0 is the characteristic timescale for the formation of a self-similar solution, which is roughly equal to the time for the external shock to start to decelerate. For $t > t_0$, the bulk Lorentz factor of the fireball scales with time as $\Gamma^2 \propto t^{-m}$, with m and κ' connected by $\kappa' = m - 3$, and $m = 3$ for an adiabatic blast wave expanding in a constant density medium. In the observer frame, the arrival time at the detector T is related to that in the fixed (laboratory) frame t by $dT = (1 - \beta)dt$, and $T = \int_0^t (2\Gamma^2)^{-1} dt \approx t/[2(m + 1)\Gamma^2]$ (Fenimore et al. 1999). The differential energy conservation relation in the observer frame is now given by $dE/dT = \mathcal{L}_{BZ}(T/T_0)^q - \kappa(E/t)$, and the integrated relation is

$$E = \frac{\mathcal{L}_{BZ}}{\kappa + q + 1} \left(\frac{T}{T_0}\right)^q T + E_{\nu\bar{\nu}} \left(\frac{T}{T_0}\right)^{-\kappa}, \quad T > T_0. \quad (16)$$

Here $\mathcal{L}_{BZ} = 2\Gamma^2(t_0)L_{BZ}$, and $q = (q' - m)/(m + 1)$, $\kappa = \kappa'/(m + 1)$. Since $\kappa + q + 1 = (q' + \kappa' + 1)/(m + 1)$, the comparisons between q and $-\kappa - 1$ in the following discussion are equivalent to the comparisons between q' and $-\kappa' - 1$. At different times, the total energy of the blast wave may be dominated either by a continuous injection term or by the initial impulsive term (Zhang & Mészáros 2001, and references therein). Which of the two is dominant at a particular observation time T depends both on the values of the two indices (q and $-\kappa - 1$), and on the relative values of \mathcal{L}_{BZ} and $E_{\nu\bar{\nu}}$. If $q < -1 - \kappa$, the impulsive term always dominates since the first term is negative. For an adiabatic blast wave expanding in a constant density medium (i.e. $m = 3$ and $\kappa = \kappa' = 0$), this condition yields $q' < -1$. If $q > -1 - \kappa$, the continuous term will eventually dominate (i.e. $E_{\nu\bar{\nu}} \ll \mathcal{L}_{BZ}T_0$) over the

second term after a critical time

$$T_c = T_0 \times \max \left[1, \left((\kappa + q + 1) \frac{E_{\nu\bar{\nu}}}{\mathcal{L}_{BZ}T_0} \right)^{1/(\kappa+q+1)} \right]. \quad (17)$$

This is the case considered in many pulsar central engines (Usov 1992, 1994; Dai & Lu 1998). We then have $T_c \approx T_0$ and the fireball is completely analogous to the impulsive regime with $E_{\text{total}} \approx \mathcal{L}_{BZ}T_0$.

If initially $E_{\nu\bar{\nu}} \gg \mathcal{L}_{BZ}T_0$, the critical T_c after which the continuous injection becomes dominant could be much longer than T_0 , exerting a noticeable influence on the GRB afterglow. We expect this to be the case either when the magnetic energy is below equipartition ($\rho c_s^2 > B^2/8\pi$) or when the timescale for the formation of a self-similar solution is small ($T_0 \ll T_c$). Because of the strong pinch that develops, a narrow jet that delivers its thrust in a narrow solid angle, Ω_{BZ} , may be a common ingredient of strong rotating magnetic fields (see Meier, Koide & Uchida (2001) for a recent review). We thus generally expect the magnetic outflow to be much more collimated than that produced by $\nu\bar{\nu}$ annihilation ($\Omega_{BZ} \ll \Omega_{\nu\bar{\nu}}$) and the magnetic luminosity to be the dominant contribution. Even in this case, the impulsive term $E_{\nu\bar{\nu}}$ may be responsible for either creating a cavity before the magnetized wind expands or for precursor emission. The detection of, or strong upper limits on, such features would provide constraints on the burst progenitor and on magnetar-like central engine models.

An external shock can occur at much larger radii and over a much longer timescale than in usual afterglows, if the environment has a very low density. This may be the case for GRBs arising from compact binary mergers that are ejected from the host galaxy into an external medium that is much less dense than the ISM assumed for usual models (where the particle density is $n \sim 0.1 - 1 \text{ cm}^{-3}$). It is commonly assumed that compact mergers occur outside the host galaxies because of the long inspiral, due to the emission of gravitational waves. We note that recent calculations of evolutionary tracks of binary systems containing massive stars show that the merger events can occur on much shorter timescales and thus still within the host galaxy, because the initial binary separation is small (Belczynski, Bulik & Kalogera 2002).

Our simulations would indicate that the central engine survives the initial, violent event that created it, and that it possesses enough energy to account for the energetics and durations of short GRBs. However, they clearly cannot tackle directly other relevant issues, mainly related to the evolution of the magnetic field, and its influence on the dynamics. Magnetic instabilities could make the disk lifetime much shorter by effectively increasing the viscosity. The amplification of the magnetic field may be self-limiting due to magnetic

stress, which would cause disk flaring. The properties of the expected variability depend strongly on the details of the configuration of the disk corona generated by the magnetic field, which is removed from the disk by flux buoyancy (Narayan, Paczyński & Piran 1992; Tout & Pringle 1996; Kluźniak & Ruderman 1998).

It is a pleasure to acknowledge many helpful conversations with W. Kluźniak, D. Lazdazi, G. Ogilvie, D. Price, M. J. Rees, S. Rosswog and V. Usov. We thank the referee for his comments and suggestions for improvements to the text. WHL thanks the IoA for its hospitality. Financial support for this work was provided in part by CONACyT (27987E), PAPIIT (IN-110600), SEP and the Royal Society.

REFERENCES

- Abramowicz, M. A., Calvani, M. & Nobili, L. 1983, *Nature*, 302, 597
- Abramowicz M. A., Karas V., Lanza A. 1998, *A& A*, 331, 1143
- Balbus, S. A. & Hawley, J. F. 1991, *ApJ*, 376, 214
- Balbus, S. A. & Hawley, J. F. 1998, *Rev. Mod. Phys.*, 70, 1
- Balsara, D. 1995, *J. Comp. Phys.*, 121, 357
- Belczynski, K., Bulik, T., Kalogera, V. 2002, *ApJ*, 571, L147
- Bildsten, L. & Cutler, C. 1992, *ApJ*, 400, 175
- Blandford, R. D. & McKee, C. F. 1976, *Phys. Fluids*, 19, 1130
- Blandford, R. D. & Znajek, R. L. 1977, *MNRAS*, 179, 433
- Cohen, E., Piran, T. & Sari R. 1998, *ApJ*, 509, 717
- Connaughton, V. 2002, *ApJ*, 567, 1028
- Dai, Z. G., & Lu, T. 1998, *Phys. Rev. Lett.*, 81, 4301
- Daigne, F. & Mochkovitch, R. 1997, *MNRAS*, 285, L15
- Eichler, D., Livio, M., Piran, T. & Schramm, D. N. 1989, *Nature*, 340, 126
- Fenimore, E. E., Cooper, C., Ramirez-Ruiz, E., Sumner, M. C. 1999, *ApJ*, 512, 683
- Fenimore, E. E., Ramirez-Ruiz, E. & Wu, B. 1999, *ApJ*, 518, L73
- Flebbe, O., Münzel, S., Herold, H., Riffert, H. & Ruder, H. 1994, *ApJ*, 431, 754
- Font, J. A. & Daigne, F. 2002, *MNRAS* in press (astro-ph/0203403)
- Hawley, J. F. 2000, *ApJ*, 528, 462
- Hawley, J. F. & Balbus, S. A. 1991, *ApJ*, 376, 223
- Hawley, J. F. & Krolik, J. H. 2001, *ApJ*, 548, 348
- Hawley, J. F. & Krolik, J. H. 2002, *ApJ*, 566, 164
- Hulse, R. A. & Taylor, J. H. 1975, *ApJ*, 195, L51

- Igumenshchev, I. V. 2000, MNRAS, 314, 54
- Igumenshchev, I. V., Chen, X. & Abramowicz, M. A. 1996, MNRAS, 278, 236
- Igumenshchev, I. V. & Abramowicz, M. A. 1999, MNRAS, 303, 309
- Igumenshchev, I. V. & Abramowicz, M. A. 2000, ApJS, 130, 463
- Igumenshchev, I. V., Abramowicz, M. A. & Narayan, R. 2000, ApJ, 537, L27
- Kalogera, V., Narayan, R., Spergel, D. N. & Taylor, J. H. 2001, ApJ, 556, 340
- Katz, J. & Canel, L. M. 1996, ApJ, 471, 915
- King, A. 1995, in X-ray binaries, eds. W. H. G. Lewin, J. van. Paradijs, E. P. J. van den Heuvel, Cambridge University Press, p.419
- Kita, D. 1995, Ph. D. Thesis, University of Wisconsin–Madison
- Kley, W. & Lin, D. N. C 1992, ApJ, 397,600
- Kluźniak, W. & Kita, D. 2000, astro-ph/0006266
- Kluźniak, W. & Lee, W. H. 1998, ApJ, 494, L53
- Kluźniak, W. & Ruderman, M. 1998, ApJ, 505, L113
- Kochanek, C. S. 1992, ApJ, 398, 234
- Kohri, K. & Mineshige, S. 2002, submitted (astro-ph/0203177)
- Kouveliotou, C., Meegan, C. A., Fishman, G. J., Bhat, N. P., Briggs, M. S., Koshut, T. M., Paciesas, W. S. & Pendleton, G. N. 1993, ApJ, 413, L101
- Lattimer, J. M. & Prakash, M. 2001, ApJ, 550, 426
- Lattimer, J. M. & Schramm, D. N. 1976, ApJ, 210, 549
- Lazzati, D., Ramirez-Ruiz, E. & Ghisellini, G. 2001, A&A, 379, L39
- Lee, W. H. & Kluźniak, W. 1999a, ApJ, 526, 178
- Lee, W. H. & Kluźniak, W. 1999b, MNRAS, 308, 780
- Lee, W. H. 2000, MNRAS, 318, 606
- Lee, W. H. 2001a, MNRAS, 328, 583, (L01)

- Lee, W. H. 2001b, *ApSS*, 276, 239
- Lu, Y., Cheng, K. S., Yang, L. T. & Zhang, L. 2000, *MNRAS*, 314, 453
- MacFadyen, A. I. & Woosley, S. E. 1999, *ApJ*, 524, 262
- Masuda, N., Nishida, S. & Eriguchi, Y. 1998, *MNRAS*, 297, 1139
- McKinney, J. C. & Gammie, C. F. 2002, *ApJ* in press (astro-ph/0204045)
- Meier, D. L., Koide, S. & Uchida, Y. 2001, *Science*, 291, 84
- Mészáros, P. 2001, *Science*, 291, 79
- Mészáros, P. & Rees, M. J. 1997, 482, L29
- Mochkovitch, R., Hernanz, M., Isern, J. & Martin, X. 1993, *Nature*, 361, 236
- Monaghan, J. J. 1992, *ARAA*, 30, 543
- Monaghan, J.J. & Lattanzio, J.C. 1985, *A&A*, 149, 135.
- Nakar, E. & Piran, T. 2002, *MNRAS*, 330, 920
- Narayan, R., Paczyński, B. & Piran, T. 1992, *ApJ*, 395, L83
- Narayan, R., Piran, T. & Kumar, P. 2001, *ApJ*, 557, 949
- Norris, J. P., Nemiroff, R. J., Bonnell, J. T., Scargle, J. D., Kouveliotou, C., Paciesas, W. S., Meegan, C. A. & Fishman, G. J. 1996, *ApJ*, 459, 393.
- Nishida, S., Lanza, A., Eriguchi, Y. & Abramowicz, M. A. 1996, *MNRAS*, 278, L41
- Nishida, S. & Eriguchi, Y. 1996, *ApJ*, 461, 320
- Paczyński, B. 1986, *ApJ*, 308, L43
- Paczyński, B. 1991, *Acta. Astron.*, 41, 257
- Paczyński, B. & Wiita, P. J. 1980, *A&A*, 88, 23
- Piran, T. 1999, *Phys. Rep.*, 314, 575
- Popham, R., Woosley, S. E. & Fryer, C. 1999, *ApJ*, 518, 356
- Pringle, J. E. 1981, *ARAA*, 19, 137

- Ramirez-Ruiz, E. & Fenimore, E. 2000, ApJ, 539, 712
- Rees, M. J. & Mészáros, P. 1992, MNRAS, 258, 41P
- Rees, M. J. & Mészáros, P. 1994, ApJ, 430, L93
- Rees, M. J. 1999, A&AS, 138, 491.
- Rosswog, S. & Davies M. B. 2002, MNRAS in press (astro-ph/0110180)
- Ruffert, M. & Janka, H.-T. 1999, A& A, 344, 573
- Salpeter, E. E. 1964, ApJ, 140, 796
- Sari, R. & Piran, T. 1997, ApJ, 485, 270
- Shakura, N. I. & Sunyaev, R. A. 1973, A&A, 24, 337
- Stone, J. M., Pringle, J. E. & Begelman, M. C. 1999, MNRAS, 310, 1002
- Stone, J. M. & Pringle, J. E. 2001, MNRAS, 322, 461
- Tout, C. A. & Pringle, J. E. 1996, MNRAS, 281, 219
- Urpin, V. 1984, Sov. Astr. Letters, 28, 50 (Astron. Zh. 61, 84)
- Usov, V. V. 1992, Nature, 357, 472
- Usov, V. V. 1994, MNRAS, 267, 1035
- Wilson, D. B. 1984, Nat., 312, 620
- Woosley, S. E. 1993, ApJ, 405, 273
- Zel'dovich, Ya. B. 1964, Sov. Phys. Dokl., 9, 195 (Dokl. Akad. Nauk, 155, 67)
- Zhang, B. & Mészáros, P. 2001, ApJ, 552, L35

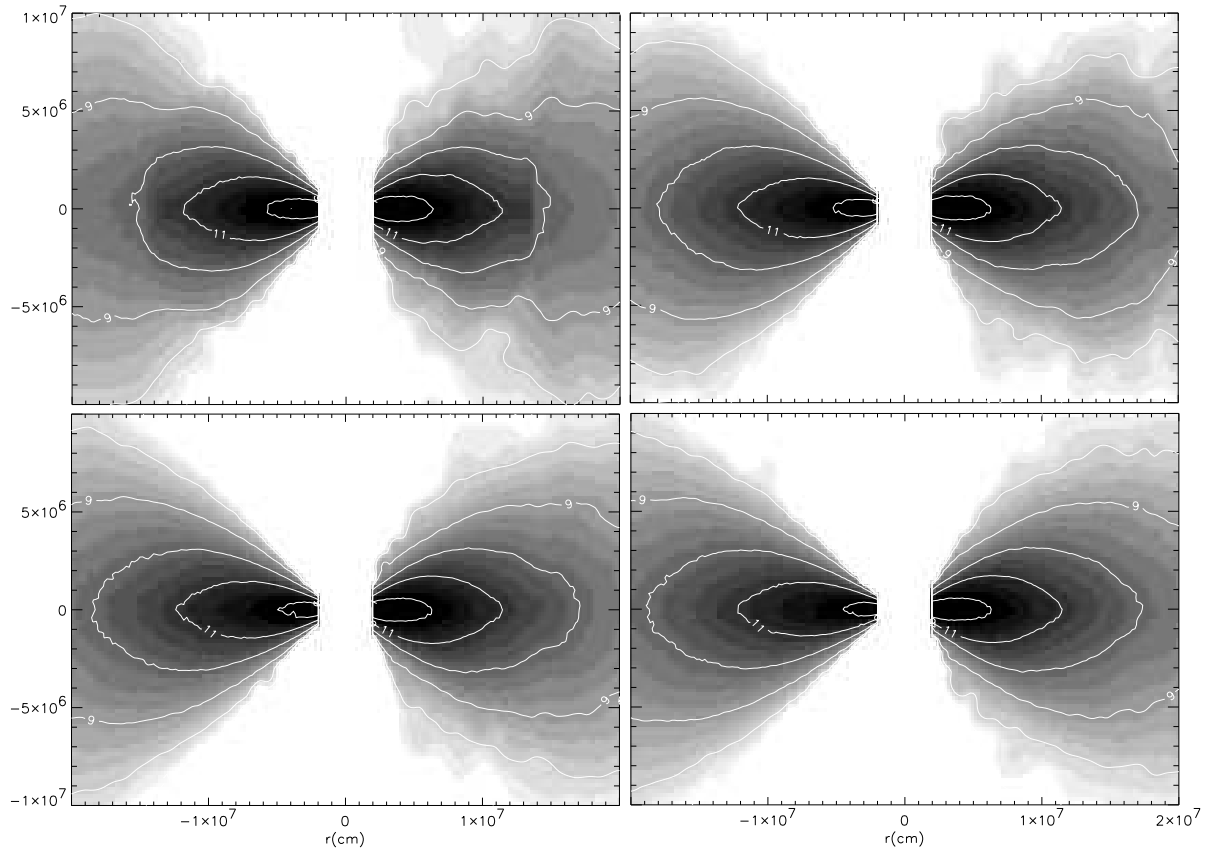


Fig. 1.— Logarithmic density contours (equally spaced and labeled in g cm^{-3}) at $t = 10$ ms (top left), $t = 20$ ms (top right), $t = 30$ ms (bottom left) and $t = 40$ ms (bottom right) for runs E and G. In each panel, the left half ($r < 0$) corresponds to run E ($\alpha = 0.1$) while the right half ($r > 0$) corresponds to run G ($\alpha = 0.01$).

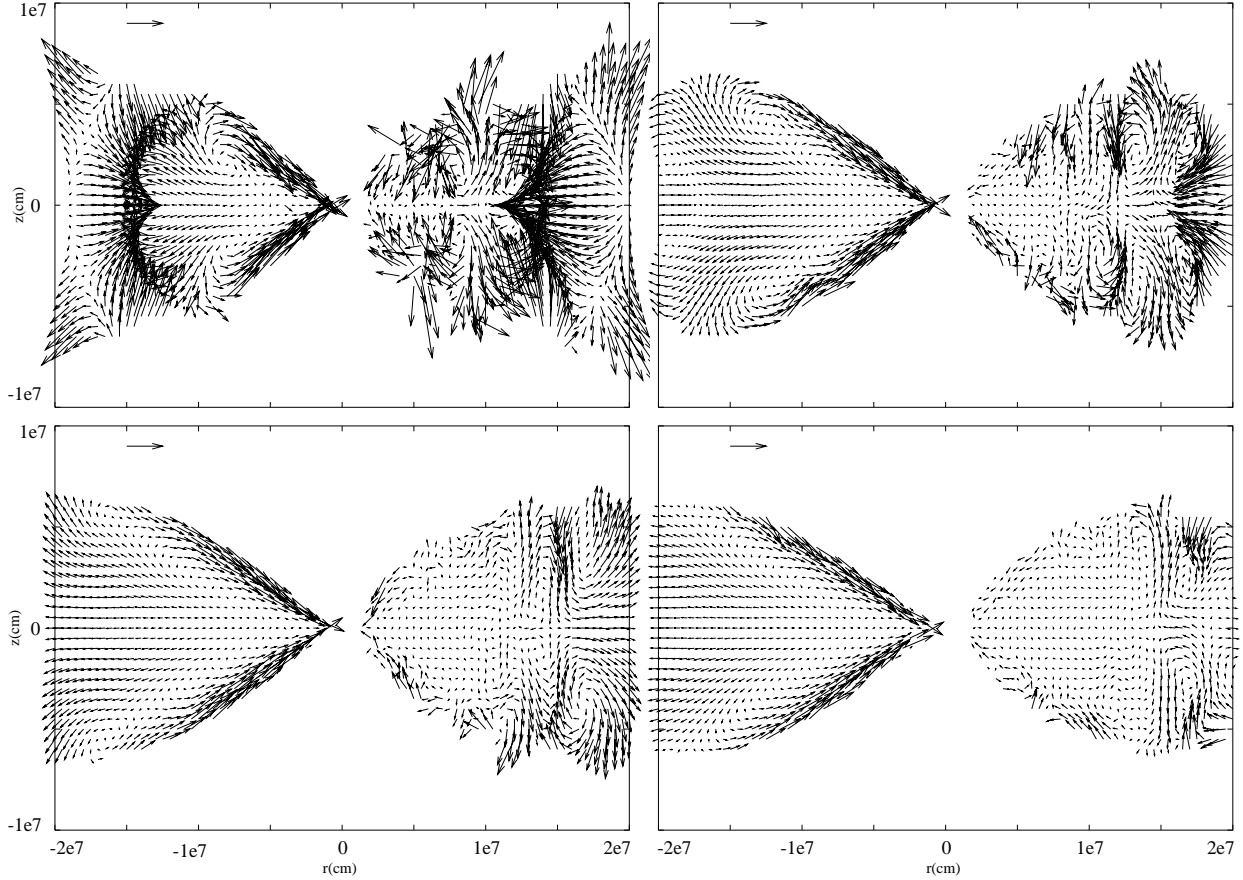


Fig. 2.— Same as Figure 1 but showing the velocity field. The equatorial outflow at large radii, and the inflow along the surface of the disk can be clearly seen, particularly for run E (left half of each panel). Note the small-scale eddies present in run G in every panel. The strength of the circulation diminishes in time, but does not die out. The velocity field is only shown if $\rho > 6 \times 10^8 \text{ g cm}^{-3}$ for clarity (in these panels the edge of the disk, as given by the SPH particle distribution extends to lower densities, by about one order of magnitude, see Figure 1). The vector in the top left corner of each panel has magnitude $v = 5 \times 10^8 \text{ cm s}^{-1}$.

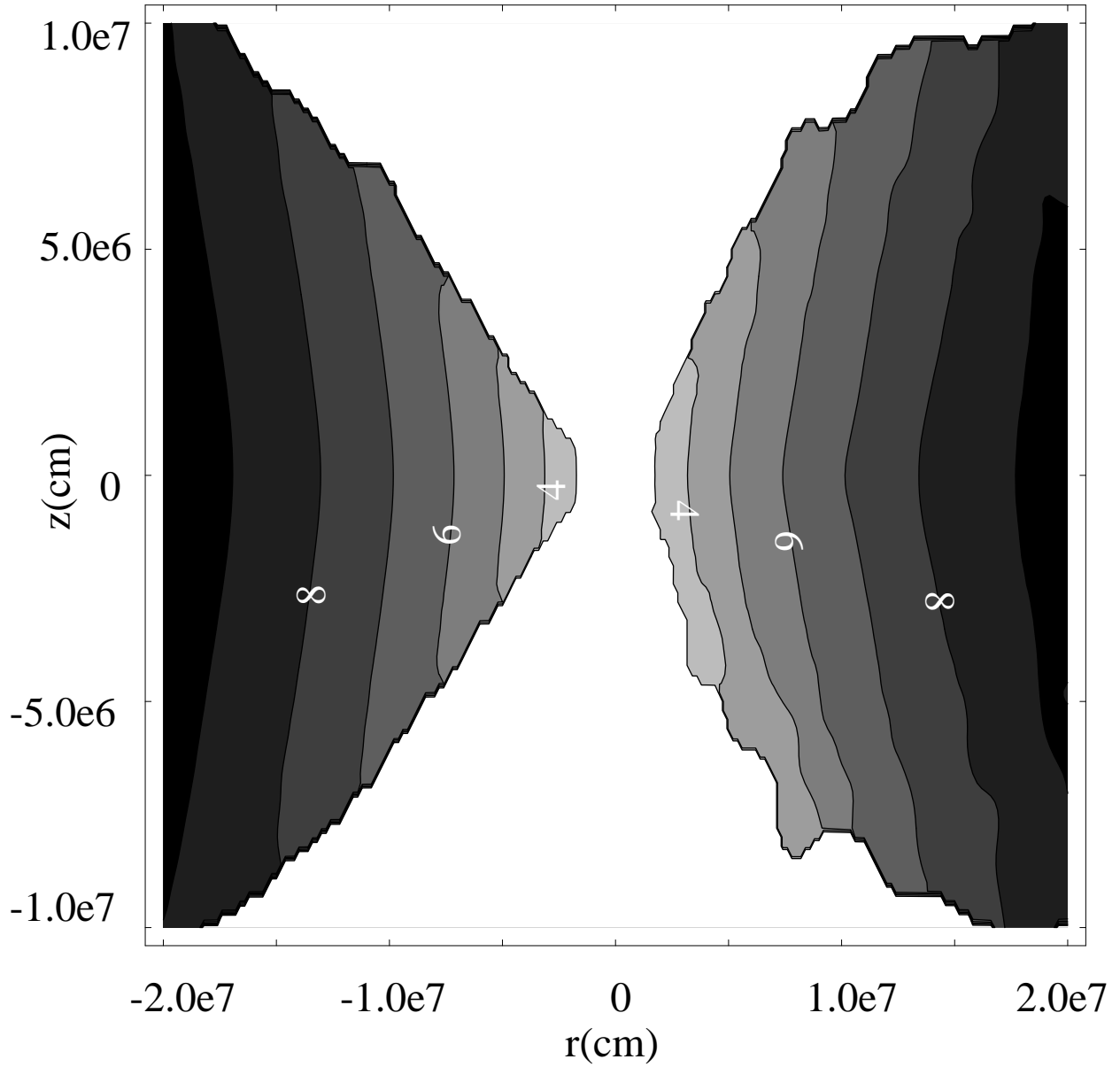


Fig. 3.— Contours of specific angular momentum l for runs E ($\alpha = 0.1$) and G ($\alpha = 0.01$) at $t = 40$ ms (corresponding to the last panel in Figures 1 and 2). The left half of the panel ($r < 0$) corresponds to run E, and the right half ($r > 0$) to run G. The contours are equally spaced and the labels correspond to $l/10^{16} \text{ cm}^2 \text{ s}^{-1}$.

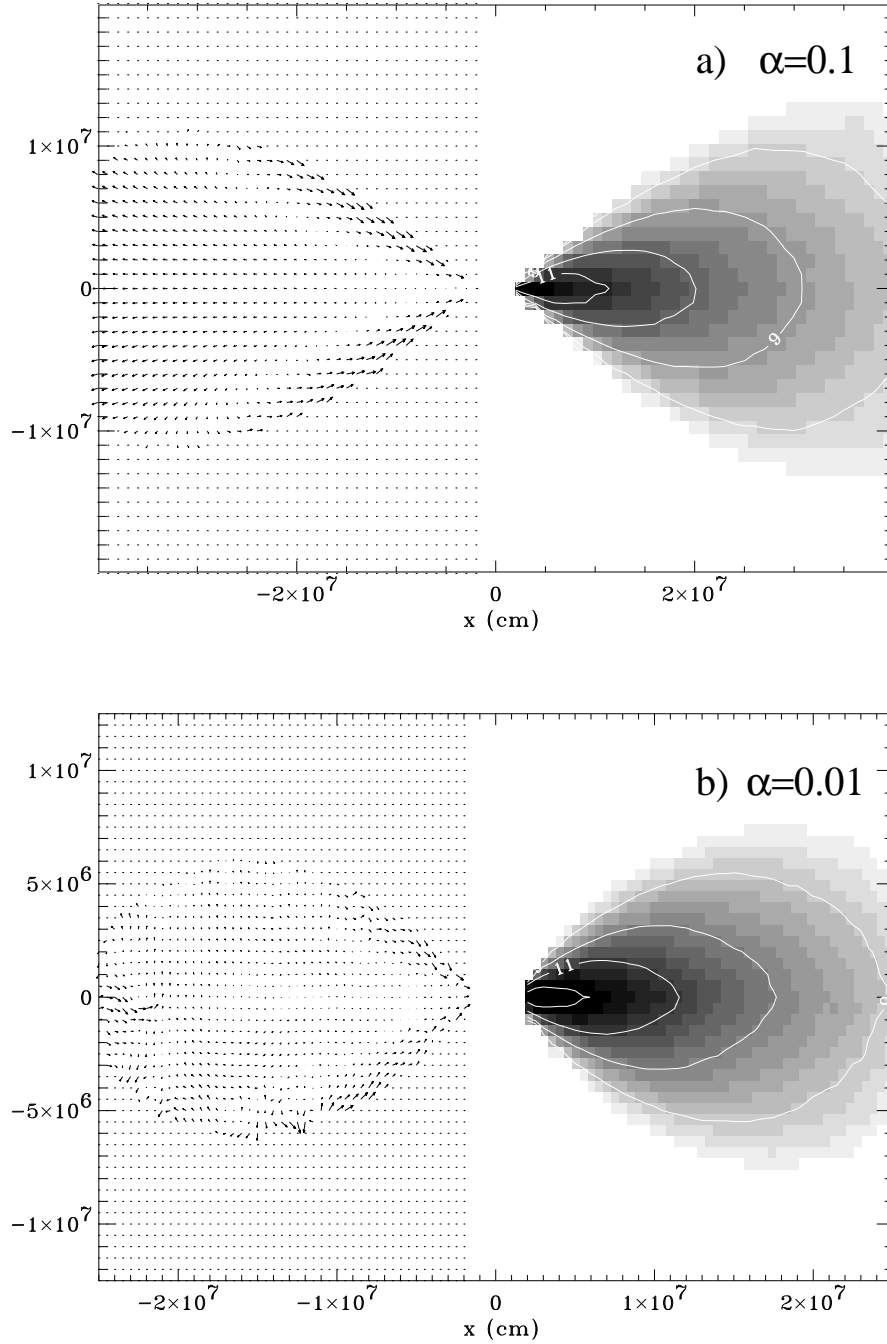


Fig. 4.— Logarithmic density contours (equally spaced and labeled in g cm^{-3}), and velocity field for run E (a) and G (b) at $t = 0.11 \text{ s}$. Note the different scales on the axes for each panel. The longest arrows correspond to $v = 2.9 \times 10^8 \text{ cm s}^{-1}$ for (a) and $v = 10^8 \text{ cm s}^{-1}$ for (b).

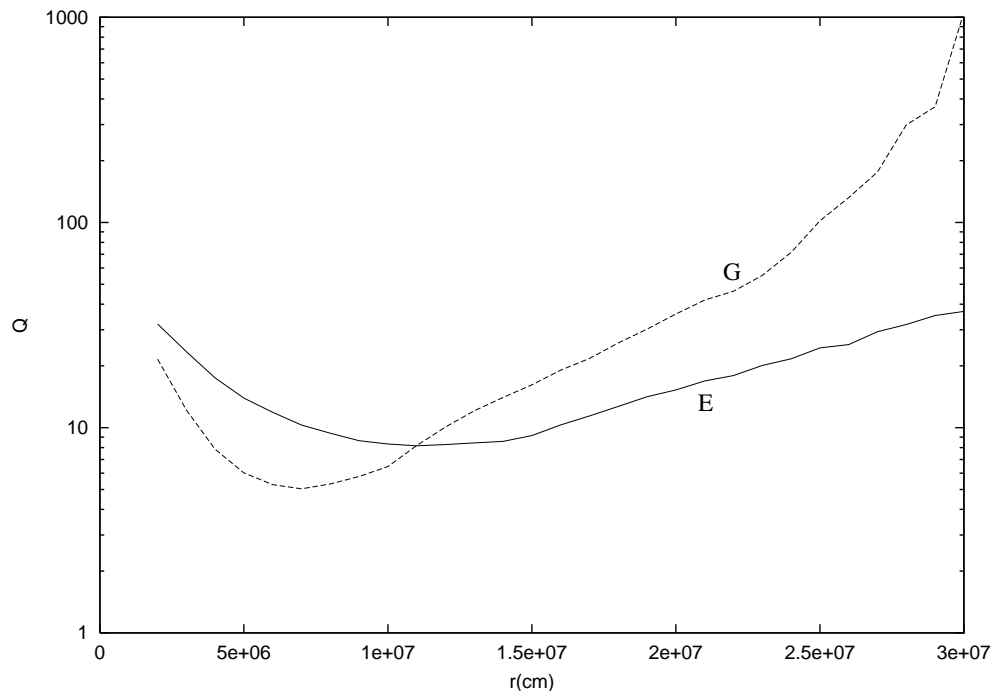


Fig. 5.— Toomre stability parameter Q as a function of the radial coordinate r for runs E (solid line, $\alpha = 0.1$) and G (dashed line, $\alpha = 0.01$), at $t = 0.1$ s.

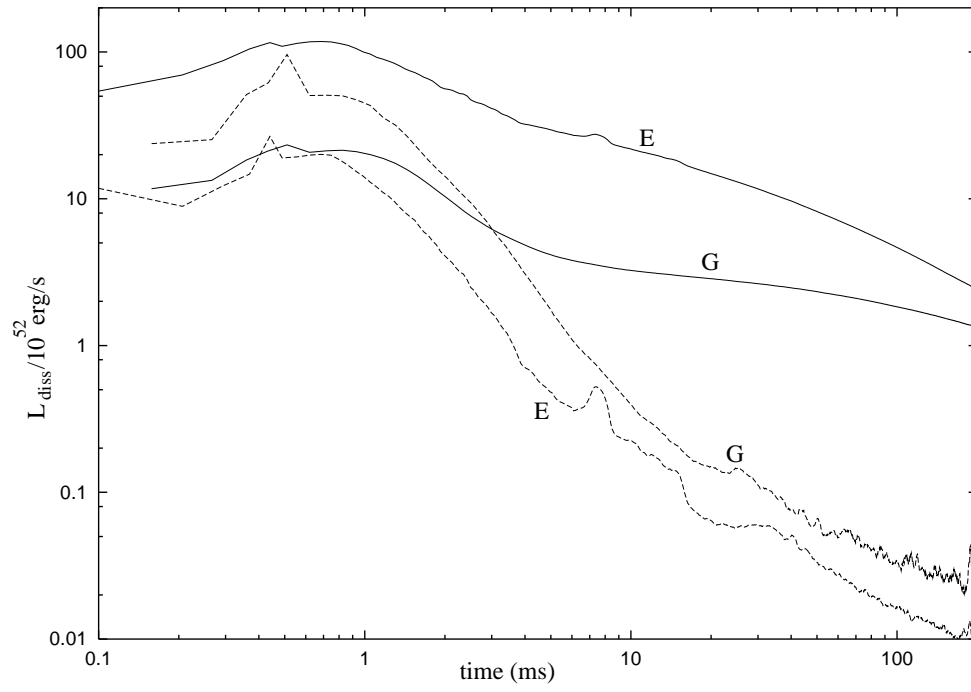


Fig. 6.— Energy dissipation rate as a function of time for runs E and G arising from the stress tensor $t_{\alpha\beta}$ (solid lines, L_ν), and from artificial viscosity (dashed lines).

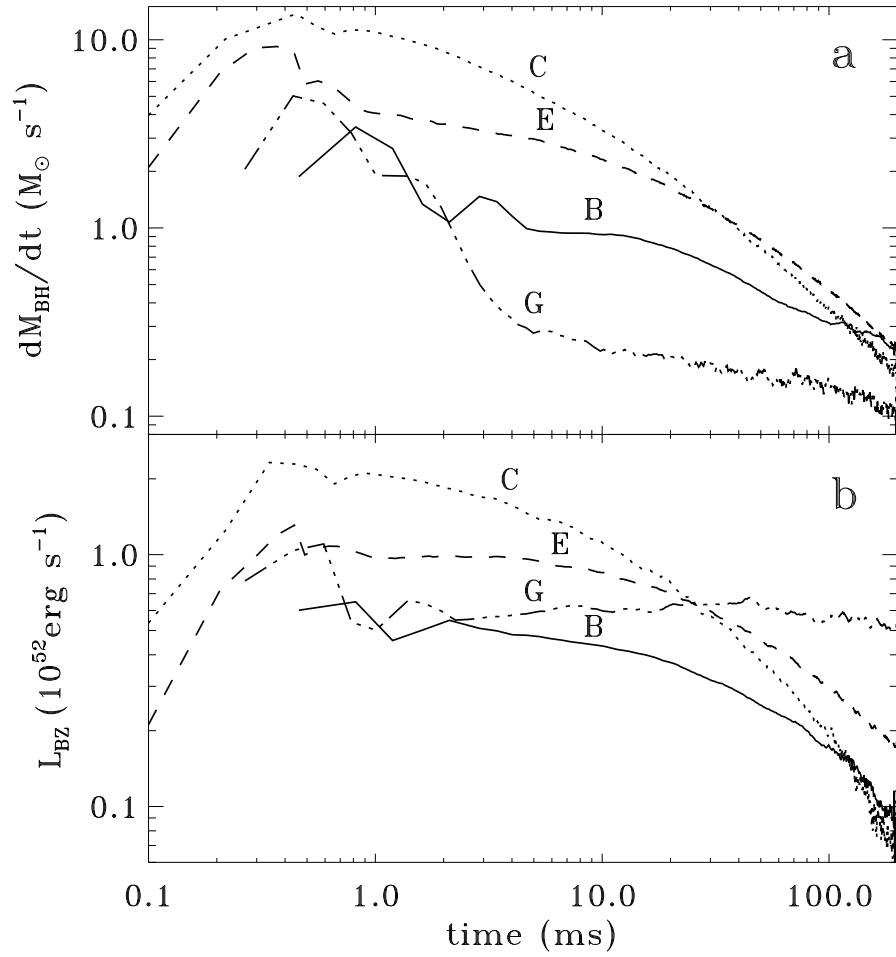


Fig. 7.— (a) Accretion rate (in solar masses per second) onto the black hole for runs B, C, E and G. (b) Blandford–Znajek luminosity L_{BZ} for the same runs as shown in (a).

Table 1. Initial conditions for the accretion disks.

| Run | q_b ^a | Γ | α | M_{BH}/M_{\odot} ^b | $M_{\text{disk}}/M_{\odot}$ ^b | N ^c |
|-----|--------------------|----------|----------|--|--|------------------|
| A | 0.31 | 2.0 | 0.1 | 5.57 | 0.266 | 21,609 |
| B | 0.31 | 4/3 | 0.1 | 5.57 | 0.266 | 21,609 |
| C | 0.50 | 2.0 | 0.1 | 3.85 | 0.308 | 19,772 |
| D | 0.50 | 4/3 | 0.1 | 3.85 | 0.308 | 19,772 |
| E | 0.50 | 4/3 | 0.1 | 3.85 | 0.308 | 79,489 |
| F | 0.50 | 4/3 | 0.01 | 3.85 | 0.308 | 19,772 |
| G | 0.50 | 4/3 | 0.01 | 3.85 | 0.308 | 39,658 |

^aMass ratio $q_b = M_{\text{NS}}/M_{\text{BH}}$ of the original binary system used in the three-dimensional simulation.

^bValues at the start of the two-dimensional calculation of the accretion disk evolution.

^cNumber of SPH particles at the start of the two-dimensional calculation.

Table 2. Accretion disk parameters during the dynamical evolution.

| Run | $\dot{M}/(M_{\odot}/s)^a$ | $\rho c_s^2/(\text{erg cm}^{-3})^a$ | $L_{\nu}(\text{erg s}^{-1})^a$ | $E_{\nu}(\text{erg})^b$ | $L_{BZ}(\text{erg s}^{-1})^a$ | $E_{BZ}(\text{erg})^b$ | M_{disk}/M_{\odot}^b |
|-----|---------------------------|-------------------------------------|--------------------------------|-------------------------|-------------------------------|------------------------|------------------------|
| A | 0.33 | $1.8 \cdot 10^{30}$ | $3.25 \cdot 10^{52}$ | $1.38 \cdot 10^{52}$ | $1.00 \cdot 10^{51}$ | $2.94 \cdot 10^{50}$ | 0.128 |
| B | 0.31 | $2.1 \cdot 10^{30}$ | $3.61 \cdot 10^{52}$ | $1.08 \cdot 10^{52}$ | $1.75 \cdot 10^{51}$ | $4.05 \cdot 10^{50}$ | 0.151 |
| C | 0.36 | $3.5 \cdot 10^{30}$ | $4.00 \cdot 10^{52}$ | $1.79 \cdot 10^{52}$ | $2.00 \cdot 10^{51}$ | $6.47 \cdot 10^{50}$ | 0.137 |
| D | 0.48 | $5.0 \cdot 10^{30}$ | $5.00 \cdot 10^{52}$ | $1.52 \cdot 10^{52}$ | $2.50 \cdot 10^{51}$ | $6.25 \cdot 10^{50}$ | 0.158 |
| E | 0.47 | $5.3 \cdot 10^{30}$ | $4.65 \cdot 10^{52}$ | $1.57 \cdot 10^{52}$ | $2.95 \cdot 10^{51}$ | $7.41 \cdot 10^{50}$ | 0.160 |
| F | 0.13 | $12.5 \cdot 10^{30}$ | $1.86 \cdot 10^{52}$ | $0.44 \cdot 10^{52}$ | $6.00 \cdot 10^{51}$ | $1.17 \cdot 10^{51}$ | 0.254 |
| G | 0.15 | $12.0 \cdot 10^{30}$ | $1.84 \cdot 10^{52}$ | $0.44 \cdot 10^{52}$ | $5.65 \cdot 10^{51}$ | $1.15 \cdot 10^{51}$ | 0.255 |

^aValues are given at $t = 0.1$ s.

^bValues are given at $t = 0.2$ s.